Aus dem Universitätsklinikum Münster

Klinik und Poliklinik für Nuklearmedizin

- Direktor: Univ.-Prof. Dr. Dr. Otmar Schober -

Effects of Patient Motion on Absolute Quantification of Glucose Metabolism in Cardiac Positron Emission Tomography (PET)

INAUGURAL-DISSERTATION

zur

Erlangung des doctor rerum medicinalium

der Medizinischen Fakultät

der Westfälischen Wilhelms-Universität Münster

vorgelegt von Jörg Eckardt

aus Münster

2003

Gedruckt mit Genehmigung der Medizinischen Fakultät der Westfälischen Wilhelms-Universität Münster

Dekan:	**Univ.-Prof. Dr. Heribert Jürgens**
1. Berichterstatter:	**Univ.-Prof. Dr. Dr. Otmar Schober**
2. Berichterstatter:	**Univ.-Prof. Dr. Walter Leonard Heindel**
Tag der mündlichen Prüfung:	**25.09 und 01.10.2003**

Aus dem Universitätsklinikum Münster
Klinik und Poliklinik für Nuklearmedizin
- Direktor: Univ.-Prof. Dr. Dr. Otmar Schober -

Referent: Univ.-Prof. Dr. Dr. Otmar Schober
Koreferent: Univ.-Prof. Dr. Walter Leonard Heindel

Zusammenfassung

Effects of Patient Motion on Absolute Quantification
in Cardiac Positron Emission Tomography (PET)

Jörg Eckardt

Die Positronen-Emissions-Tomographie (PET) stellt eine der leistungsfähigsten Methoden zur Bestimmung myokardialer Vitalität dar, deren Bestimmung für die Prognose und Therapie von Patienten mit koronarer Herzerkrankung elementar ist.

Ziel der vorliegenden Arbeit war es, das Auftreten und die Einflüsse von Patientenbewegung anhand von klinischen und simulierten Daten zu untersuchen. Ein numerisches Herzmodell wurde neu entwickelt, die Einflüsse von künstlichen Bewegungen auf das Modell und klinische Daten untersucht und diese Ergebnisse mit bewegungskontaminierten klinischen Daten verglichen.

Es wurde festgestellt, dass Patientenbewegung in mehr als einem Drittel der PET-Untersuchungen auftritt. Die simulierten Bewegungsartefakte zeigten gleiche Ergebnisse für das Modell und die klinischen Daten. Der Vergleich mit klinischen Bewegungsartefakten bestätigt diese Ergebnisse.

Tag der mündlichen Prüfung: 25.09 und 01.10.2003

Contents

List of Figures

List of Tables

1 Introduction

Coronary artery disease is the leading cause for mortality in the developed countries. Advances in pharmacological, interventionell, and surgical therapy (e.g. coronary revascularization and heart transplantation) help to reduce mortality in those patients. Correct assessment of the extent of viable and non viable myocardium is one key figure for clinical decision making. Detection of viability based on the assessment of glucose metabolism with **P**ositron **E**mission **T**omography (PET) is a clinical reference method [64], other methods as contrast-enhanced Magnetic Resonance Imaging [30] or echocardiography [67] are also validated approaches.

The strength of PET with ^{18}F-FDG in this field is its ability to quantify glucose metabolism in absolute numbers three dimensionally [47] whereby scanning procedures of more than 1 h are necessary [32]. Effects of patient motion during imaging procedures with long scanning times like SPECT are well known [19, 14]. Although motion in PET can be determined and corrected within some limits [28, 56, 53], patient data is rarely corrected for motion. Effects of motion-biased data on absolute quantification is assumed [34, 27] rather than investigated.

The aim of this work is the determination of patient movement which occurs unsystematically and often unrecognizable by the investigator in clinical practice. Furthermore effects of patient motion on the calculation of glucose metabolism will be analyzed. Effects on the results of absolute glu-

cose metabolism will be studied on phantom data and in a clinical setup on artificially motion-biased data. The impact of this results on the clinical work will be investigated by application of these results on patient data with and without movement correction methods.

2 Basics

2.1 Detection of Myocardial Viability

Myocardial viability is a key parameter in the selection of patients for myocardial revascularization procedures. Since electrocardiographic methods are usually not sufficient for this detection imaging procedures have to be carried out [40]. The next section will describe briefly different imaging methods for the detection of myocardial viability with their advantages and disadvantages [50].

2.1.1 Ultrasound Imaging

Dobutamine **S**tress **E**chocardiography (DSE) investigates the difference in contractility between a rest situation and pharmacologically evoked stimulation of the heart by ultrasound. It detects the contractile reserve of the heart which correlates to its physiological status [54]. Best results are provided when detecting a "biphasic response": at low pharmacological concentrations of the stress agent an improvement of contractility is detected whereas at high concentrations a hypokinesis of the investigated wall segment is evoked due to a lack of oxygen provoked by coronary stenosis [11].

Myocardial **C**ontrast **E**chocardiography (MCE) uses contrast media composed of a solution of microbubbles or occasionally air filled microspheres for blood pool marking. Assuming, that myocardial viability necessitates a preserved microcirculation and implying a preserved microvasculature MCE is

capable of detecing myocardial perfusion. Segmental wall motion and hence myocardial viability is verified on a high level [67].

2.1.2 Magnetic Resonance Imaging

Stress **M**agnetic **R**esonance **I**maging (SMRI) uses the same pharmacological approach as DSE. Due to the superior spatial resolution and a three-dimensional approach quantitative determination of contractility is possible. Nevertheless, reported specifity and sensitivity show discrepancies [11], partially explainable by different criteria. SMRI provides results for detection of myocardial viability, comparable to other methods described here. Contrast enhancement with Gd-DTPA shows promising results [46].

Magnetic **R**esonance **S**pectroscopy (MRS) is capable of accessing the chemical composition of tissue. This method is technically complex and still under development, although first results are quite promising [11]. Spatial resolution cannot compete with SMRI.

2.1.3 Positron Emission Tomography

PET in relation to the other imaging techniques is still known for the highest sensitivity in the detection of myocardial viability whereas the specifity is inferior to other methods [37, 11]. Its ability to obtain absolute values of metabolic rates is unique.

2.2 Positron Emission Tomography

Postiron Emission Tomography is a technique which is able to detect the distribution of positron-emitters three-dimensionally. In this chapter physical properties of positron decay, production of positron emitters, radioactive labelling of pharmaceuticals and analysis of PET-data will be described.

2.2.1 Positron Decay

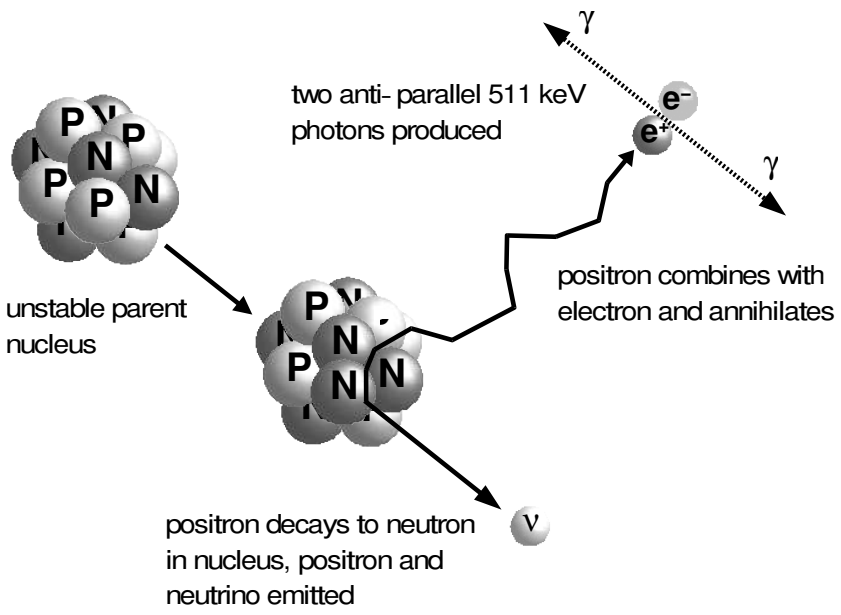

Figure 1: Principle of β^+-decay: formation of the positron (β^+-radiation) and annihilation process resulting in γ-radiation [55]. (P: proton, N: neutron, e^+: positron, e^-: electron, ν: neutrino)

Positron decay is one of the three beta decay processes. These are characterized by the transition of the charge of a nucleon. A positron or an

electron and its corresponding neutrino is generated in the nucleus. Hereby the atomic number is modified by one unit, the chemical element changes, and the mass number A is constant. In the case of the β^+-decay, the atomic number decreases by one, and the positron, describable as a positive charged electron is emitted:

$$ {}^{A}_{Z}X \longrightarrow {}^{A}_{Z-1}Y_{N+1} + e^+ + \nu_e. \tag{1} $$

The particle ν_e on the right hand side of (1) is the electronic neutrino; since it is only measurable with modern and sophisticated equipment it was initially undetectable but postulated. It has no direct effect on any part of the PET-equipment; only its involvement in the decay reaction results in a statistical distribution of the reaction energy over the three emitted particles. With no neutrino involved the energy would be distributed to the nucleus and the positron exactly with respect to their masses.

As visualized in figure 1 the emitted positrons are slowed down by interactions with the electrons in matter. Positrons are counted among antimatter; if the energy degradation is sufficient, the positron reacts with its anti-particle, the electron, leading to an annihilation process [31].

2.2.2 Production of Radiopharmaceuticals with a Cyclotron

Physical and Biochemical Characteristics of Radiopharmaceuticals

A radiopharmaceutical is a pharmaceutical with a radioactive entity. It may be seen from two points of view affecting each other: the physical one, dealing with the nuclear characteristics of the emitting atom and on the other hand the biochemical one, taking the chemical characteristics, the behavior in a human organism with all its metabolic processes into account.

From the physical point of view the limitations affect the choice of the radiating atom in the chemical bond:

- type of emitted radiation: since absorption for pure α- and β^--radiation in tissue is high, γ-emitting nuclides are used for **S**ingle **P**hoton **E**mission **C**omputed **T**omography (SPECT) and PET.

- energy of emitted radiation: absorption for γ-emitting nuclides in tissue is strongly depending on their energy; suitable for imaging purposes are only those with an energy between 70 keV and 511 keV.

- half-life of the radiopharmaceutical: it must be long enough to make the imaging process possible resulting in a minimum half-life of about 60 s. From the radiation protection point of view, the half-life must be as short as possible, limiting the half-life of the usable nuclides for human diagnostic purposes to a few hours.

Positron-emitting radionuclides can be produced with a cyclotron or via a generator-system. The choice is not totally free and depends mostly on the individual nuclide desired.

From the biochemical point of view, the limitations result from the desire to visualize the metabolic process of the radiopharmaceutical similar or equal to a physiological one, or at least characteristic for it:

- good uptake in tissue
- no metabolic processes except from the desired ones

Although many radiation-emitting nuclides are known, the number of usable ones is quite limited with respect to physical and biochemical issues. Both points of view are mostly addressed by labelling pharmaceuticals with positron emitters produced with a cyclotron. Hence it will be described in the next chapter.

Isotope	half-life [min]	Maximum positron energy [MeV]	Mean positron range in water [FWHM im mm]	Production method
^{11}C	20.3	0.96	0.85	cyclotron
^{13}N	9.97	1.19	1.15	cyclotron
^{15}O	2.03	1.72	1.8	cyclotron
^{18}F	109.8	0.64	0.46	cyclotron
^{68}Ga	67.8	1.90	2.15	generator
^{82}Rb	1.26	3.35	4.1	generator

Table 1: Properties of commonly used radio-isotopes [3, 7, 6]

Production of Positron Emitters with a Cyclotron

Since the half-life of the presented positron emitters is short, they are not found in nature. Positron emitters are characterized by being rich in protons; therefore the aim of any production method is the enrichment of positive charge in a nucleus. The only direct access is the transport of protons (positively charged) into the nucleus. The Coulomb-force repels the similarly charged proton and the nucleus from each other. This long-range repulsive force must be overcome to bring the protons in the (low-range) reach of the nuclear force which keeps the proton inside the nucleus. Hence the proton must be accelerated to high velocities (mostly expressed in units of energy, ranging in a few MeV) which is possible with different particle accelerators [38]. Mostly, cyclotrons are used for the production of high energy protons, hence its function will be described briefly.

The acceleration of particles on a non-linear spiral way was invented in 1932 [33], its principle delineated in figure 2. It consists of an ion source placed in the middle of the 4 dees (electrodes) all situated in a high-vacuum. Each dee consists of two (one upon the other) electrically connected plates where adjacent dees are also electrically connected (same color in figure 2). A large electric coil is depicted only by the resulting magnetic field.

A negatively charged hydrogene-ion (proton with 2 electrons) is emitted radially from the negatively charged ion source. Entering the region of the dees it is repelled from the negatively charged dee in counter-clockwise direction (depicted black) and attracted from the positively charged (depicted

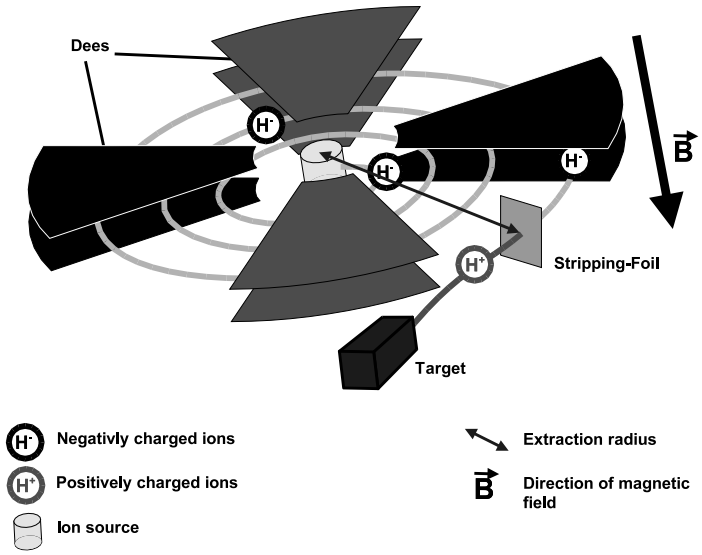

Figure 2: Principles of a cyclotron

grey) in clockwise direction. In the moment the ion passes through the two plates of the dee in the clockwise direction (depicted grey) the polarity of the dees is changed. After passing the ion is again repelled from the now negatively charged dee in counter-clockwise direction and attracted from the positively charged in clockwise direction The spiral pathway in this process is caused by the magnetic field: the Lorentz-Force effects perpendicular to the direction of movement of the charge particle and the magnetic flux lines, in direction of the centre of the spiral. Since it is not large enough to compensate the centrifugal force fully the radius of the ion's pathway increases. By high frequent change of the electric polarity of the dees the ion is accelerated further on. When the ion passes the stripping foil, the 2 electrons are pulled

of the ion and a proton remains, travelling further on. Thereby the Lorenz-Force effects in the radial direction driving the proton out of the acceleration field into the target. Target reactions depend on the energy of the incident proton and the target filling-material. One possible reaction is

$$^{18}O + p \longrightarrow ^{18}F + n. \tag{2}$$

A full description with the exact physical derivation can be found in [59] the coverage of substantially questions of radiation protection in this field in [15, 24].

Radioactive Labelling of Pharmaceuticals

Once a radioactive nuclide is produced, a pharmaceutical is to be labelled with it. Since PET-radiochemistry is a complex field only the key demands should be addressed here shortly, an introduction can be found in [49, 58].

- A basic need is a fast labelling process in units of the half-life of the radioactive nuclide used. The layout of the synthesis is chosen best, when the radioactive labelling is conducted late in the synthesis.

- Many applications like imaging neurotransmitters or enzymes require radiotracers with high specific activities. Though chemistry with smallest amounts of substances (nanomolar quantities) requires sophisticated planning of reactions

- Due to the short half-life, quality control of the radiopharmaceutical cannot be performed for all currently accepted ones before application. Basic tests are conducted before, quality control is performed according to legal regulation additionally including control of starting materials, stability tests, tests after application (e. g. for sterility and apyrogenity).

- The activities handled are high (range of GBq) implying a high radiation level. To address radiation protection issues radiochemistry must be widely remotely controlled and performed in lead-shielded gas-tight hot-cells.

The mostly used PET-tracer also used in this thesis is 2-**F**luoro(18)-2-**D**eoxy-D-**G**lucose (FDG) as shown in figure 3 and its clinical role is extensively investigated [22].

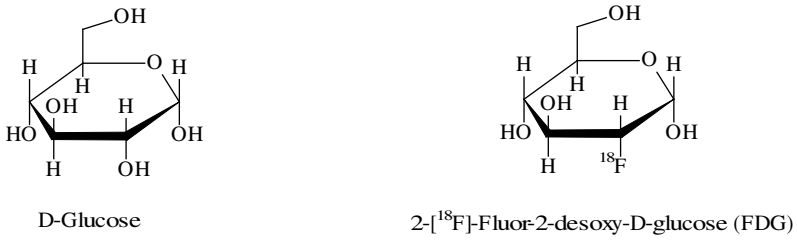

Figure 3: Structure responsible for different biochemical pathways (chapter 2.2.4): 2-Fluoro(18)-2-Deoxy-D-Glucose (right) differs from D-Glucose (left) only in the replacement of the hydroxyl group on the second carbon atom.

2.2.3 Positron Emission Tomograph

The key issue in scintigraphic imaging is not only to detect an ionizing particle but also to receive information about its origin. A Positron Emission Tomograph is principally designed as shown in figure 4. Many small scintillators (approx. 10000) are placed on a ring around the field of view. Each detector element is optically connected with an electronic device able to detect the γ-quants emitted at the annihilation process of a positron. Since the time of travelling is short it can be assumed, that two γ-quants, detected in a short time-window (in the range of 10 ns), belong to the same annihilation process. The origin of emission and hence the place of annihilation lies somewhere on the direct line between these two detectors (LOR= **L**ine **O**f **R**esponse). The so-called coincidence detection is visualized in figure 4: only events detected in both channels are assumed to originate frome one annihilation process and are selected for the imaging process.

PET-data is biased by different effects which are corrected for:

- Attenuation in the tissue: this effect is corrected by a transmission scan provided by rotating radioactive sources [65, 61] or alternatively by a CT system [29].

- Random coincidences, caused by two γ-quants emitted by different annihilation incidences and being accidently identified as being coincident [9].

- Scatter is evoked by one of the 2 coincident detected γ-quants being

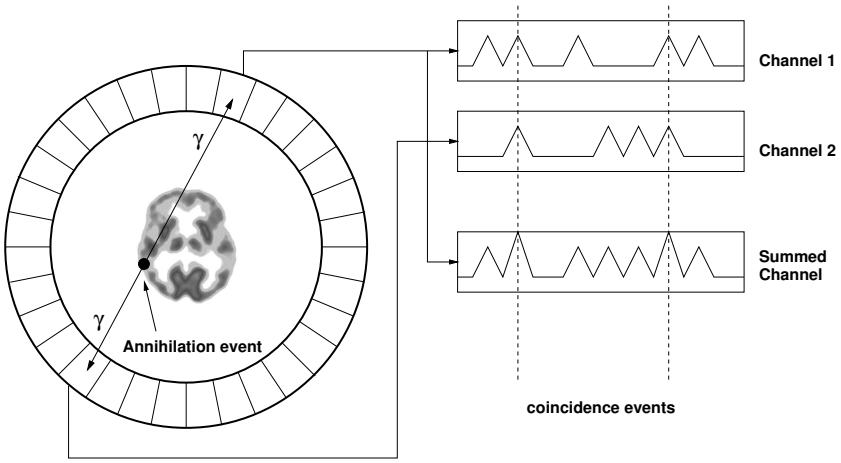

Figure 4: Coincidence detection in a PET-scanner [55]

scattered in tissue and resulting in a false LOR [66, 2].

- Dead time occurs since the detectors have a limited count rate capability; γ-quants irradiating one detection element in high frequency (scale of ms^{-1}) cannot be differentiated by this detection element [8].

- Different sensitivities of different LORs are evoked by different sensitivity of the detection elements themselves and geometric reasons [43].

After a mathematical reconstruction with respect to these corrections has been carried out, the activity concentration in every point in the field of view is obtainable with respect to the resolution of the system.

2.2.4 Kinetic Model of 2-Fluoro(18)-2- Deoxy-Glucose (FDG)

The reconstructed data-set from the PET-scanner only gives information about the physical three-dimensional distribution of the radioactive nuclide injected to the patient. Combination of this physical data with information about the metabolic pathway of the injected radiopharmaceutical is nesccessary. In this chapter the fundamentals of the FDG-model are delineated. Details and their appliance to cardiac investigations can be found in [26, 47, 57].

Compartment Model

In the description of the compartmental model the difference between FDG and D-glucose as depicted in figure 3 is important. The model used in this work is a three-compartment model, the principle of which is visualized in figure 5. All constants and variables concerning the radioactive FDG are marked with an asterisk (e.g. k_1^*, C_p^*), those for the natural analogon without (e.g. k_1, C_p).

FDG is injected into a vein and thus distributed over the capillary system of the whole body and reaches the myocardium. FDG in blood plasma is defined as the first compartment. FDG is transported into the tissue by the same transporter as glucose. The transport constant characterizing this process for FDG is k_1^*, for the reverse transport k_2^*. Qualitatively, the metabolic process for glucose and FDG is similar in the next step: FDG and glucose are phosphorylized by the hexokinase reaction to FDG-6-phosphate and glucose-6-phosphate respectively; the reaction is characterized for FDG with

the constant k_3^*, the backward reaction by k_4^*. At this point the metabolic pathway of glucose and FDG diverges: glucose-6-phosphate is isomerized to fructose-6-phosphate and metabolized further the glycolytic and tricarboxylic pathway. The isomerization of FDG is not possible due to the lack of the hydroxyl group on its second carbon atom (figure 3). Hence FDG is trapped in this compartment.

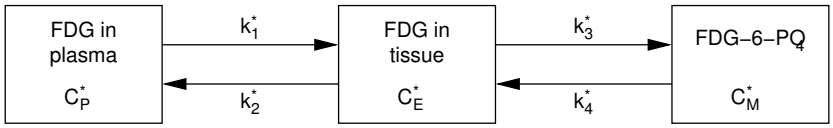

Figure 5: Three-compartment model of the metabolic process of 2-Fluoro(18)-2-Deoxy-D-Glucose.

The model used makes the following assumptions:

- Glucose metabolism is in a steady state. The metabolic rate of glucose and concentrations of all the substrates and intermediates of the glycolytic pathway are constant during the time of the study
- Concentrations of glucose, FDG and FDG-6-P are small, are homogenous in their compartments
- Concentrations of FDG and FDG-6-P are small relative to their natural counterparts so that the presence of FDG and FDG-6-P does not affect the steady-state environment of glucose metabolism.

- The transport constants of FDG and FDG-6-P between compartments have first-order kinetics.
- Tissue extraction fraction of glucose and FDG from plasma is small. In other words, the transporters of glucose and FDG to local myocardial tissue is not flow limited.

Using these assumptions an equation can be formulated which describes the glucose consumption R_i in dependency of the transport constants of FDG

$$R_i = \frac{1}{LC} \cdot \frac{k_1^* \cdot k_3^*}{k_2^* + k_3^*} \cdot C_p, \tag{3}$$

whereby LC is the "Lumped Constant" representing a calibration factor between the glucose and FDG transport. The concentration of glucose in blood C_p is simply achievable from a single blood sample whereas the derivation of the transport constants is performed by means of a PET measurement.

Determination of Absolute Glucose Metabolism

Under these assumptions, a formula describing the dependency of the activity concentration C_i^* in tissue from the plasma concentration $C_p^*(t)$ and the transport constants k_1^*-k_4^* can be written as [26]

$$C_i^*(t) = \frac{k_1^*}{\alpha_2 - \alpha_1}((k_3^* + k_4^* - \alpha_1) \cdot e^{-a_1 t} +$$

$$(\alpha_2 - k_3^* - k_4^*) \cdot e^{-\alpha_2 t}) \otimes \mathrm{C}_p^*(t), \tag{4}$$

$$with\ \alpha_{1,2} \quad = \quad \frac{k_2^* + k_3^* + k_4^* \mp \sqrt{(k_2^* + k_3^* + k_4^*)^2 - 4k_2^* k_4^*}}{2}.$$

How far k_4^* has to be taken into account is not treated on a standard way. Some publication do this [26] others do not [57]. Here the formula for $k_4^* \neq 0$ is presented.

Disregarding the back reaction of the phosphorylization reaction ($k_4^* = 0$) formula 4 may be simplified to

$$C_i^*(t) = \frac{k_1^* \cdot k_3^*}{k_2^* + k_3^*} \cdot \int_0^t C_p^*(\tau) d\tau + \frac{k_1^* \cdot k_3^*}{k_2^* + k_3^*} e^{-(k_2^* + k_3^*)\tau} \cdot \int_0^t C_p^*(\tau) \cdot e^{(k_2^* + k_3^*)\tau} d\tau \tag{5}$$

The main task of FDG-PET in absolute quantification of glucose metabolism is the determination of the transport constants k_1^*-k_4^*. Since activity concentration in tissue C_i^* and in plasma C_p^* is known a numerical solution of equation 4 (iterative) and 5 can be found.

Patlak Plot

Looking at data obtained late in the acquisition process, the change of C_p^* in comparison to this of the exponential function can be disregarded. This can be written as the linear equation [23, 44]

$$\underbrace{\frac{C_i^*(t)}{C_p^*(t)}}_{y} = \underbrace{\frac{k_1^* \cdot k_3^*}{k_2^* + k_3^*}}_{a} \cdot \underbrace{\frac{\int_0^t C_p^*(\tau)d\tau}{C_p^*(t)}}_{x} + \underbrace{\frac{k_1^* \cdot k_2^*}{(k_2^* + k_3^*)^2}}_{b} \tag{6}$$

C_p^* is obtainable from blood sample data, C_i^* from the reconstructed acquisition data. Plotting x and y with respect to the axis results in a straight with the slope of a and a y-axis interception of b (figure 6). The slope of the plot can be directly inserted into the equation (3).

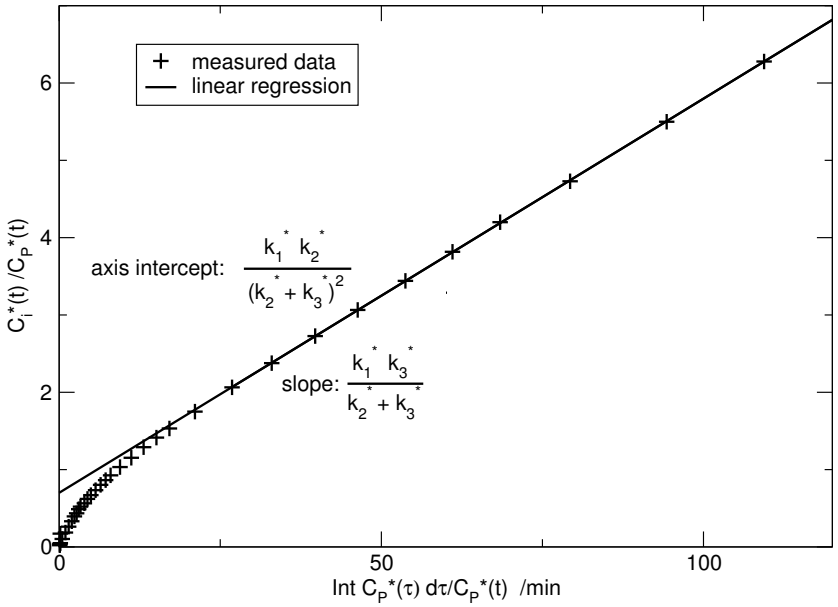

Figure 6: Patlak Plot

2.2.5 Motion

Influence of Motion and Misalignment

Motion in cardiac imaging can be divided in three types: motion due to normal cardiac exercise of the heart, respiratory motion and patient motion at a certain point of the investigation (e.g. related to uncomfortably positioning of the patient). The first two types of motion may be treated with means of cardiac or respiratory gating and are not investigated in this work.

The third type of motion (further on referred to as patient motion) is not characterizable in a systematic way since it differs in its timing and dimension from patient to patient and occurs randomly. It is known as a serious problem in cardiac nuclear medicine investigations and has been described in the literature. Results for ^{201}Tl-SPECT were obtained on patient data [18, 17, 12, 19], phantom studies, simulated data [51, 16] or a combination of these [5, 12]; an overview may be found in [19, 14]. ^{201}Tl-SPECT-studies had shown, that motion appears in 17 - 25 % of the cardiac ^{201}Tl-investigations [51, 5, 21, 20].

In contrast, data on motion effects in cardiac PET is rare: this might be explained by the key difference of SPECT an PET acquisitions: performing multi-frame PET acquisition on a dedicated PET-scanner results in one blurred frame which must not take effect on the diagnosis if only visual or static semi-quantitative methods are used; contrarily SPECT acquisitions will be affected wholly. Since the resolution of PET-acquisitions is higher

and the acquisition time is longer, motion might be present more often.

Motion in between one acquisition frame results in different effects on the reconstructed image, as loss of resolution and image artifacts in SPECT [19]. Conducting multi-frame acquisitions, inter-frame movement does not have such serious effects on every single reconstructed frame except the one within which the movement happened but might have serious effects on modelling approaches.

Motion Detection and Correction

A basic need for overlay-techniques in inter-modality comparison of tomographic information is the right alignment of the 2 datasets which is comparable with a motion estimation and correction algorithm. Image registration is mostly applied in this field and has been widely evaluated and described. General overviews of medical image registration can be found in [36] and [25] the coverage in nuclear medicine in [28]. Also video-camera-based approaches are published [48, 45].

3 Aim

Aim of this thesis is the development of a dynamic software phantom for evaluation of spatial influences on absolute quantification in cardiac PET. This validity of the software phantom is validated on a special topic of spatial influences, patient motion. This is conducted in 3 steps:

1. Clinical relevance: the relevance of the investigation is determined; the occurrence of motion (patient data) in a clinical setup will be analyzed.

2. Validation I: movement will be simulated for phantom data. The results will be validated with artificially moved patient data.

3. Validation II: the results of simulation will be further validated by comparison with motion-corrected clinical data.

4 Material and Methods

4.1 Registration and Correction of Patient Motion

Since few of the voxels of a given image contains relevant myocardial information the motion registration process needs data preprocessing. A binary coding of the image was performed (analogue to [60]) where every pixel over a certain threshold was coded as 1 all others as 0.

Different methods for image registration are known and also tested in nuclear imaging [42]. For the purposes of this work the simple but fast method similar to the **S**um of **A**bsolute **D**ifferences (SAD)[60] was used:

$$a_{lmn} = \frac{1}{N^3} \sum_{i=1}^{N} \sum_{j=1}^{N} \sum_{k=1}^{N} \left(x_{ijk} - y_{i+l,\, j+m\, k+n}\right)^2, \tag{7}$$

where N is the side length of the cubic volume in pixels, a_{lmn} is the sum over the square of intensity differences of all pixels, the original one (represented by x_{ijk}) and the shifted one (represented by $y_{i+l,\, j+m\, k+n}$; l,m,n shifts in x,- y-, z- direction respectively).

Since the Patlak Model is applicable to the later frames of the acquisition, only those frames were investigated in the image registration process. The correction method was applied on adjacent frame: the n-th ($n \in [27; 36]\, n \in \mathbb{N}$) frame was compared with the $n+1$ th. The SAD-algorithm was stopped, when a local minimum of a_{lmn} was found. Registration was evaluated in steps of whole pixels to avoid resampling artifacts. Results of the SAD algorithm

were visually controlled.

The presented method registrates only translational movement. Motion correction was performed by application of the results of the registration process on the biased dataset using standard transformations.

4.2 Software Phantom

4.2.1 Geometry of the Software-Phantom

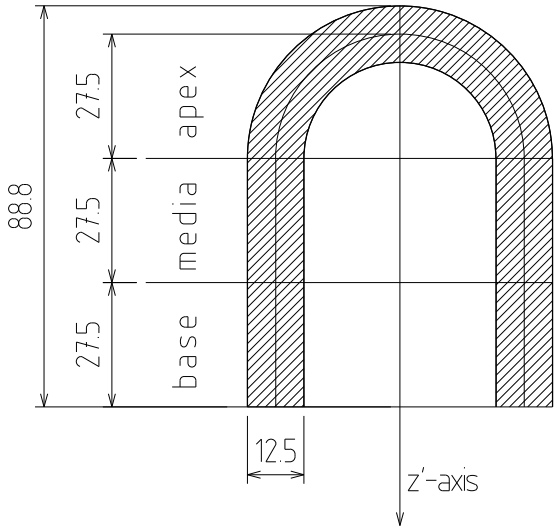

Figure 7: Geometrical shape of the heart phantom developed according to anatomical findings; the myocardium is hatched, all units are given in mm

For the simulation of motion effects and motion correction a dynamic software phantom has been developed. As shown in figure 7 the left ventricle is simulated as a combination of a cylindrical and a spherical part and matches reasonably the shape of the healthy left ventricle anatomy as shown

in figure 8. The total height of the phantom is 89 mm, the mid-myocardial diameter of the spherical and the cylindrical part 55 mm. The center of the spherical part is located in the separation plane between the spherical and the cylindrical part.

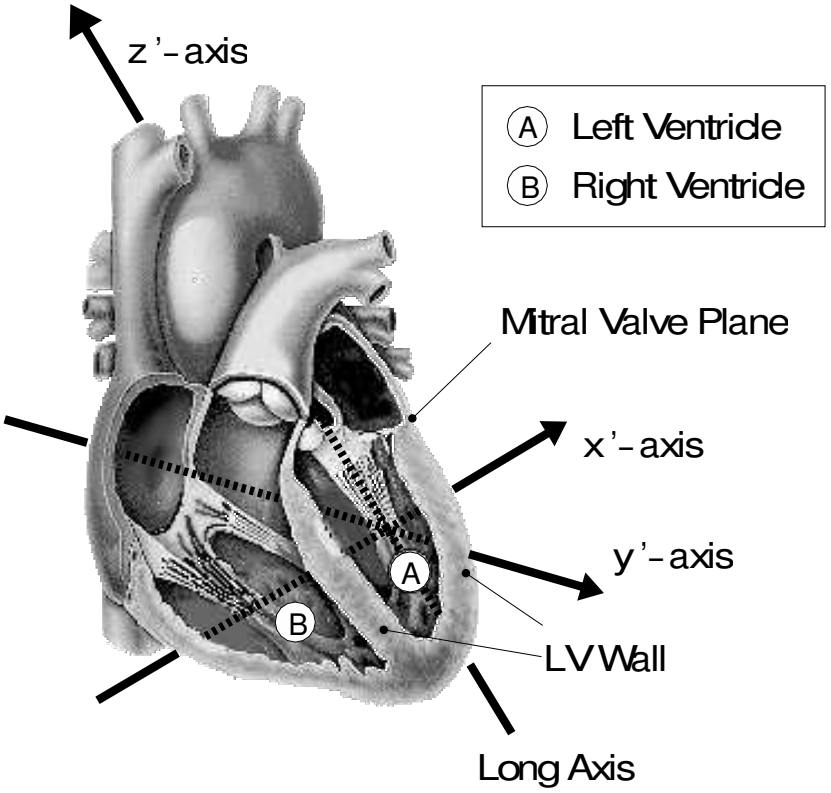

Figure 8: Anatomy of the heart and definition of the x'- and y'-axis [55].

The cylindrical part is divided into base and media, the spherical part represents the apex. In order to obtain more located information these 3 main parts are further subdivided in 4 VOIs (**V**olume **O**f **I**nterest) each. Since the septal and inferior part of base and media represent clinically differentiable

Nr.	name	shortcut	Nr.	name	shortcut
1	septal apex	Sep - A	9	inferior media	Inf - M
2	anterior apex	Ant - A	10	posterior media	Pos - M
3	lateral apex	Lat - A	11	post. septal base	Sepp - B
4	septal apex	Inf - A	12	ant. septal base	Sepa - B
5	post. septal media	Sepp - M	13	anterior base	Ant - B
6	ant. septal media	Seppa - M	14	lateral base	Lat - B
7	anterior media	Ant - M	15	inferior base	Inf - B
8	lateral media	Lat - M	16	posterior base	Pos - B

Table 2: Heart VOIs

areas, they are subdivided into two parts. The 16 different VOIs are listed in table 2.

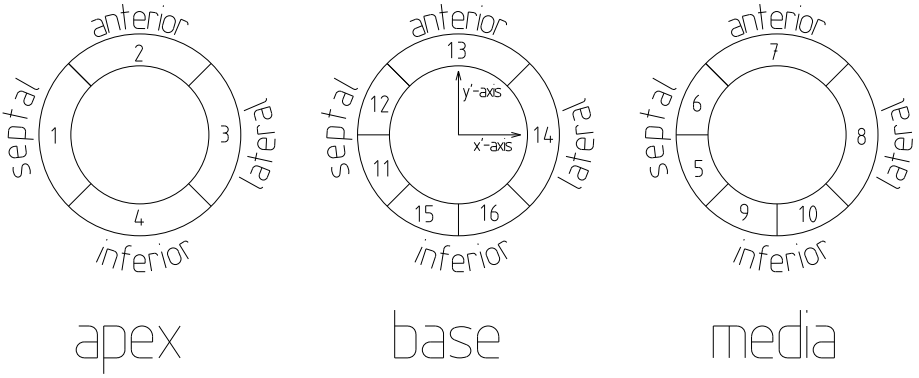

Figure 9: Segmentation of the LV and its x' and y' axis definition.

Image size (128x128x47), pixel size (2.24 mm in x- and y-direction, 3.38 mm in z-direction), and time schedule (table 3) were adjusted to the standard protocol of cardiac PET-investigations in our department.

4.2.2 Activity Levels of the Software-Phantom

The software phantom has been classified in 3 different types: inner left-ventricular volume as a blood compartment, myocardial tissue and non-myocardial tissue denominated as background.

Frame Nr.	start /s	length /s	Frame Nr.	start /s	length /s	frame Nr.	start /s	length /s
1	0	30	14	150	10	26	630	60
2	30	10	15	170	20	27	780	150
3	40	10	16	190	20	28	930	150
4	50	10	17	210	30	29	1080	150
5	60	10	18	240	30	30	1230	150
6	70	10	19	270	30	31	1380	150
7	80	10	20	300	30	32	1530	150
8	90	10	21	330	60	33	1680	150
9	100	10	22	390	60	34	1830	300
10	110	10	23	450	60	35	2130	300
11	120	10	24	510	60	36	2430	300
12	130	10	25	570	60	37	2730	300
13	140	10						

Table 3: Time schedule of a clinical FDG scan. (Injection in frame 2)

For the purposes of this work activity concentration has been calculated using a numerical backward simulation of the FDG 3K-model described in equation (5). As input curve a medium blood curve of the 10 patients was set. The average was extracted by calculating the arithmetic mean after shifting the peaks of image-derived input curves over each other. Finally, according to the compartmental model, activity levels in the phantom myocardium can be calculated by knowledge of the plasma activity concentration and the

constants k_1^*- k_3^* using equation (5).

4.2.3 Filtering and Background

Spatial resolution of a PET-scanner is limited; the exactly defined shape of the phantom was smoothed using a Gauss-Filter of the order of 7 with 7.5 mm **F**ull **W**idth at **H**alf **M**aximum (FWHM). Cardiac motion implies a volume change of the heart of about 70-80 ml. Assuming an isotropic change in volume this corresponds to a radius change of 5 mm which is simulated by additional Gaussian filtering with 5 mm FWHM. A background of 10 to 20 % were added to software phantom activity levels.

4.3 Patient Data

Data from a patient with coronary artery disease was used to evaluate the influences of motion on the absolute metabolic rate in different segments of the heart. The database for the evaluation of artificial motion contains 5 patients with an infarct and 5 patients with hibernating myocardium. These patients had been investigated in the years 1999 to 2001 in our department. This group will be referred to further on as **P**atients with **A**rtificial **M**otion (PAM).

Data of 64 patients being investigated by means of PET between 1999 and 2001 for various cardiac diseases were analyzed and corrected for patient motion. This group will be referred to as **P**atients with **C**linical **M**otion (PCM).

4.4 Simulation of Motion

Motion is difficult to evaluate in clinical data because the absolute amount of movement is not known. Hence artificial movement had to be forced and evaluated.

4.4.1 Separation of Translation and Rotation

Disregarding warping effects motion of a patient can be described mathematically as a rigid body transformation. As being a superposition of a translation and a rotation these two types of movement can be separated as visualised in figure 10.

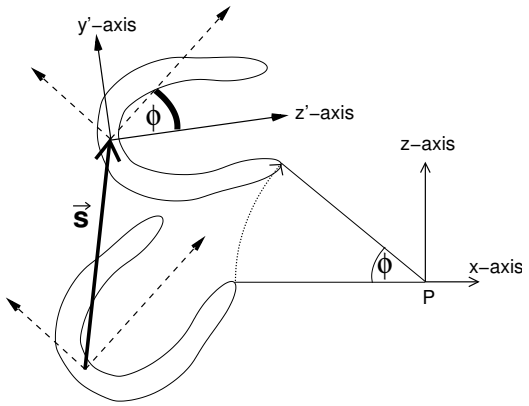

Figure 10: Visualisation of correlation between translation and rotation. The centre of rotation is P in the scanner coordinate-system, $\vec{s}$ the translational part of movement and the rotation angle ϕ. The rotation is visualised by the dotted line.

Every rotated dataset D'_{rot} in heart coordinates x', y', and z' (see figures 9 and 8) can be expressed by the product of the matrix M'_{rot} describing the

rotation multiplied with the unrotated dataset in the heart coordinates D'. The rotated dataset in scanner coordinate-system (x, y, z) D can be easily achieved when applying the inverse transformation matrix T^{-1}between the two coordinate systems:

$$\begin{aligned} D' &= T \cdot D, \\ D'_{rot} &= M'_{rot} \cdot D', \\ D_{rot} &= T^{-1} D'_{rot} = T^{-1} M'_{rot} \cdot D'. \end{aligned} \tag{8}$$

4.4.2 Simulation of Translation

The simulation of movement was performed separately for different directions. Phantom data and original image data (not reorientated, PAM group) obtained with a PET-scanner has been shifted in steps of whole pixel; shifts were simulated for the three dimensions x, y, and z describing the geometry of the PET-scanner as marked in figure 11.

4.4.3 Simulation of Rotation

Data of the software phantom and from the PAM group described in chapter 4.3 was reorientated an then rotated around the x'-, y'- and z'- axis describing the intrinsic coordinate system of the heart (see figures 9 and 8) by means of a trilinear interpolation algorithm.

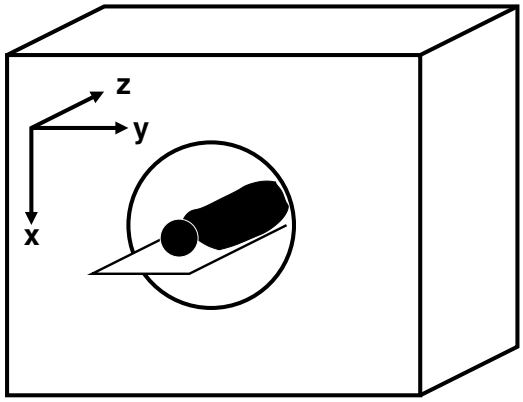

Figure 11: Definition of the x-, y-, and z-axis

4.5 PET-Scanner and Image Reconstruction

PET-Scans were performed on an ECAT Exact 921/47 (CTI, Knoxville; TN.) registering 47 planes from 24 (24 real planes and 23 interpolated) detector planes in a 15.4 cm field of view [63]. The scanner was run in 2D-mode with tungsten septa between each detector plane. Before emission, transmission scanning was performed by 3 rotating ^{68}Ge-line sources emission for 10 minutes. Emission data was collected according to the departmental time schedule also used for the software phantom (table 3).

Emission data was corrected for attenuation and detector efficiency and sorted in sinograms. For all purposes where the Patlak-Model was used reconstruction by filtered-back-projection with a cut-off at Nyquist frequency was performed. Images used for registration was reconstructed using a iterative OSEM method with 6 iterations and 16 subsets. Both methods were performed at a zoom-factor of 2.3. Pixel size in reconstructed images was

2.24 mm in x- and y-direction,and 3.38 mm in z-direction.

4.6 Quantitative Analysis of Glucose Metabolism

Patients (PAM and PCM) were investigated under the conditions of an euglycemic clamp [13, 32]. The time schedule used for the acquisition was the same as the one used for the design of the software phantom (chapter 3).

Images were reorientated, time activity curves of the blood where determined by drawing a VOI in the atrium of the left ventricle for the patient data and in the center of the left ventricle for the phantom data, corrected with late arterial samples [10]. For the software phantom, blood-sample data was extracted from the average blood curve (see chapter 4.2.2).

The unbiased dataset of the myocardium was divided in 16 VOIs using the last 3 frames. All datasets were reorientated exactly as the original (unshifted or uncorrected) datasets. Those VOIs were applied to the shifted or uncorrected datasets. All metabolic rates were calculated using the Patlak model (chapter 2.2.4). The Lumped Constant LC in equation 3 was assumed to be 1.

4.6.1 Clinical Processing

A general scheme for the classification of myocardial regions into clinically relevant groups is presented in table 4. Performing this on simulated data, each dataset is treated individually since a motion-biased dataset would be

classified clinically in between itself.

diagnosis	rel. glucose metabolism	name
scar	0 - 50 %	low
reduced metabolism	50 - 70 %	medium
normal	70 - 100 %	high

Table 4: Classification of the relative glucose consumption measured with FDG-PET in clinically relevant groups [35]. Values are presented as relative numbers in relation to the region with the maximum glucose metabolism.

The activity level of every region is calculated relatively to the region with maximal glucose metabolism. Effects of motion in this work are evaluated with a clinical scope by looking at the number of **VOI**s **c**hanging their **c**lassification (VCC) and expressed in %.

4.7 Software Issues

Image reconstruction was carried out on a SUN workstation using the ECAT 7.1 software (CTI Knoxville, TN, USA). All other data analysis was performed on standard PCs using the mathematical software package MATLAB 6 (The Mathworks Inc., MA, USA).

5 Results

5.1 Clinical Relevance: Registration of Patient Motion

Figure 12 visualizes exemplary the operation of the SAD-algorithm in a one-dimensional mode. Since the algorithm calculates principally the difference between the two images, the SAD-value decreases, when the lower image is shifted in the direction of the negative x-axis. Reaching the value of best agreement (lowest difference of the two images) the SAD-value reaches a minimum. For the purposes of this work this algorithm was conducted in a full three-dimensional mode.

Motion registration was performed on iterative reconstructed images since it worked more reliable than on images reconstructed by the filtered back-projection. 63 datasets were investigated (PCM group), motion registrated by the algorithm was recognized as patient motion when being in a range of more than one pixel. The distribution of shifts is shown in figure 13 whereas patient movement did appear often not only within one frame but was distributed over some frames.

5.2 Validation I: Simulation vs. Artificial Motion

5.2.1 Software Phantom

Patient data of 10 patients was chosen to derive k_1^*- k_3^* (nominated as k_i^*-) for the software phantom. This simulation-process is sometimes numerically

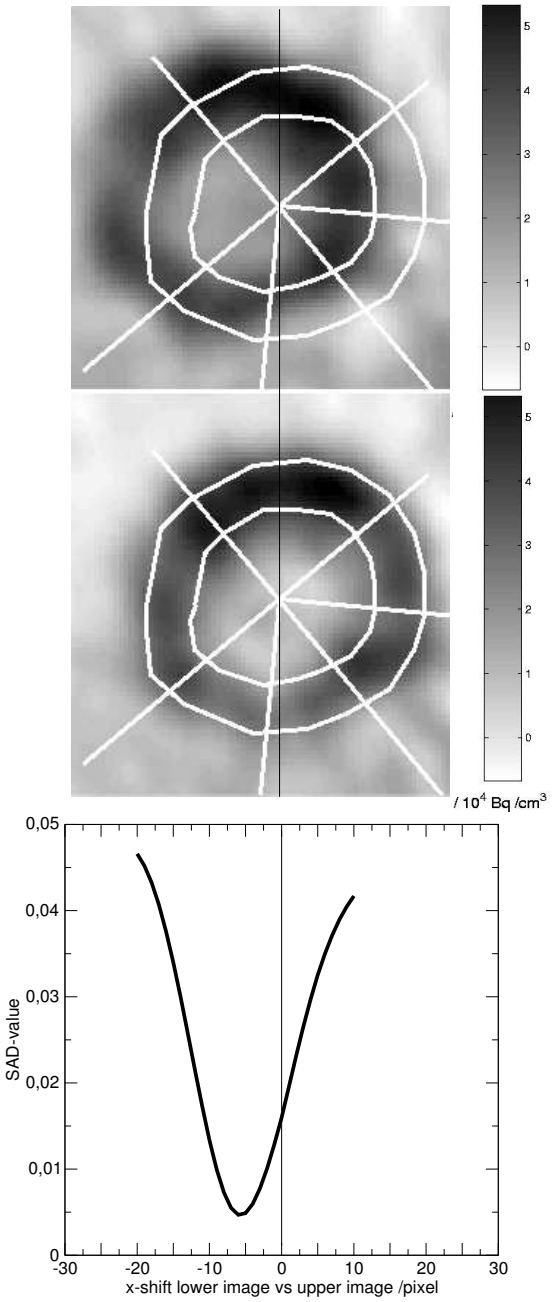

Figure 12: Operation of the registration algorithm: the regions depicted in both images are located identically.

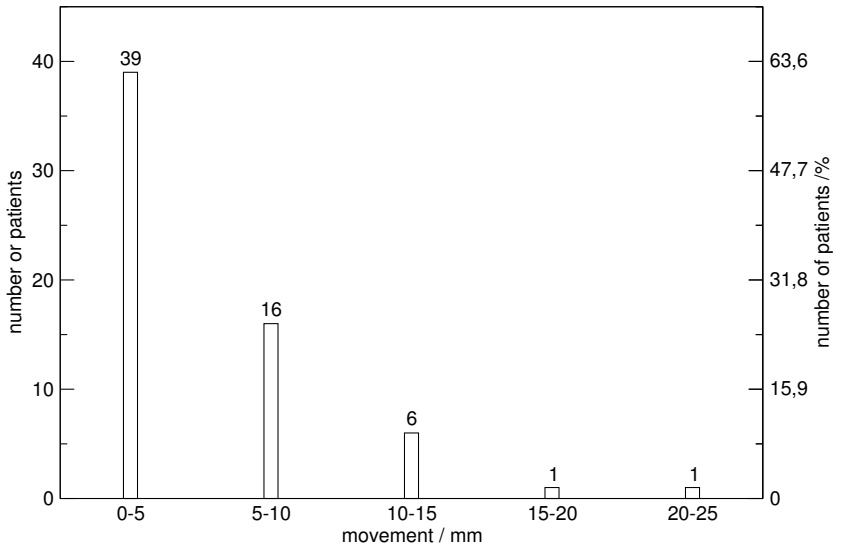

Figure 13: Results of the registration algorithm

bad-conditioned: of 160 calculated regions and their k_i^*-values those with convergence and an acceptable error rate were used. Three phantom k_i^*-sets (16 per phantom) were randomly chosen. Only their distribution over the classification ranges (see chapter 4.6.1) was prescribed to be similar to those of the patient data.

5.2.2 Translation of Phantom and Patient Data

Patient motion (PAM group) at times of 45 minutes and shifts of 10 pixels could not be simulated for every patient, since the numerical algorithm failed. 10 patients were investigated so that 320 regions were investigated for each data point. Translation was simulated from -10 to 10 pixels in steps of 2 for each dimension, resulting in shifts in the x- and y-direction of -22 mm to 22

mm in steps of 4.5 mm and -34 to 34 mm in steps of 6.8 mm in z-direction. Typical effects on Patlak-evaluations are shown in figure 14.

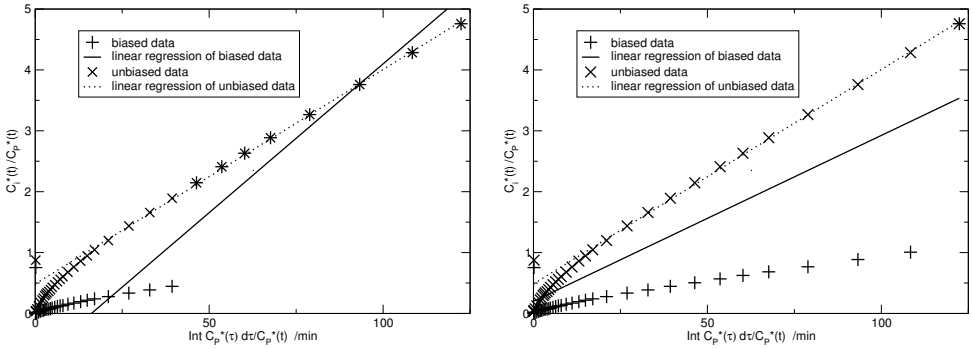

Figure 14: Effects of translation on Patlak-plot for a translation of 8 pixels in x-direction, region Inf-B: left before frame 30 (20.5 min.), right before frame 37 (40.5 min)

Starting with the anatomical phantom simulated data systematical overestimated motion effects retrieved from patient data. It was determined empirically, that next to the background level myocardial thickness is a key parameter in this simulation. Analyzing patient data, the assumption of a 12.5 mm myocardial thickness did not match clinical results of the group of 10 patients (PAM group), examples for different myocardial shapes can be found in figure 15. Selected patients of the group showed similar influences of shifts like the 12.5 mm-phantom, more precisely those with a thin myocardium. Since the myocardial thickness of a patient is impossible to characterize with a single number visual inspection was carried out. In contrast to the anatomical approach of figure 7 the data represented here has a myocardial thickness of 20 mm and represents the mean thickness of the

patient database more precisely.

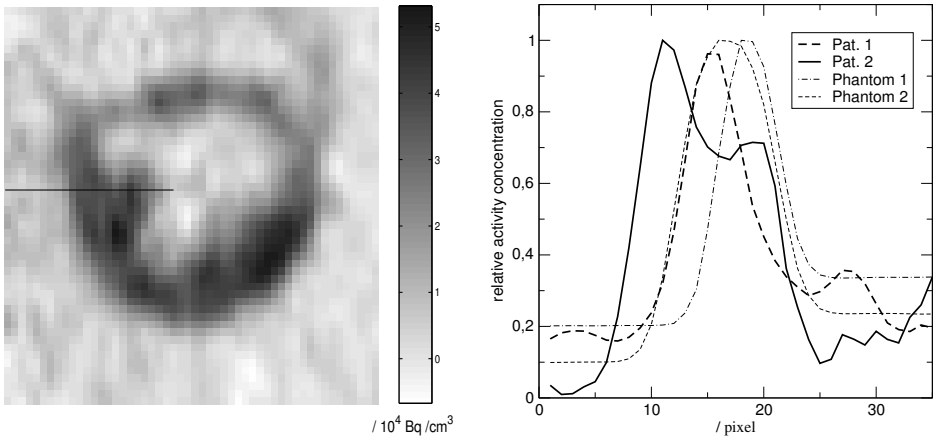

Figure 15: Effects of myocardial thickness on the line profiles of the myocardial wall (left). Comparison of the marked line profile of a thick myocardium (patient 1) with a thin myocardium (patient 2) and 2 phantoms representing different myocardial thicknesses and background levels. Colorbar values are relative.

Since 3 phantoms with 16 regions each were investigated in this figure and shifts in the positive and negative direction were summed, 96 regions were investigated.

5.2.3 Rotation of Phantom and Patient Data

Figure 17 shows data from rotation simulations. Phantom data is represented from rotations of 4° to 19° compared with one 16° rotated datasets of the patient group.

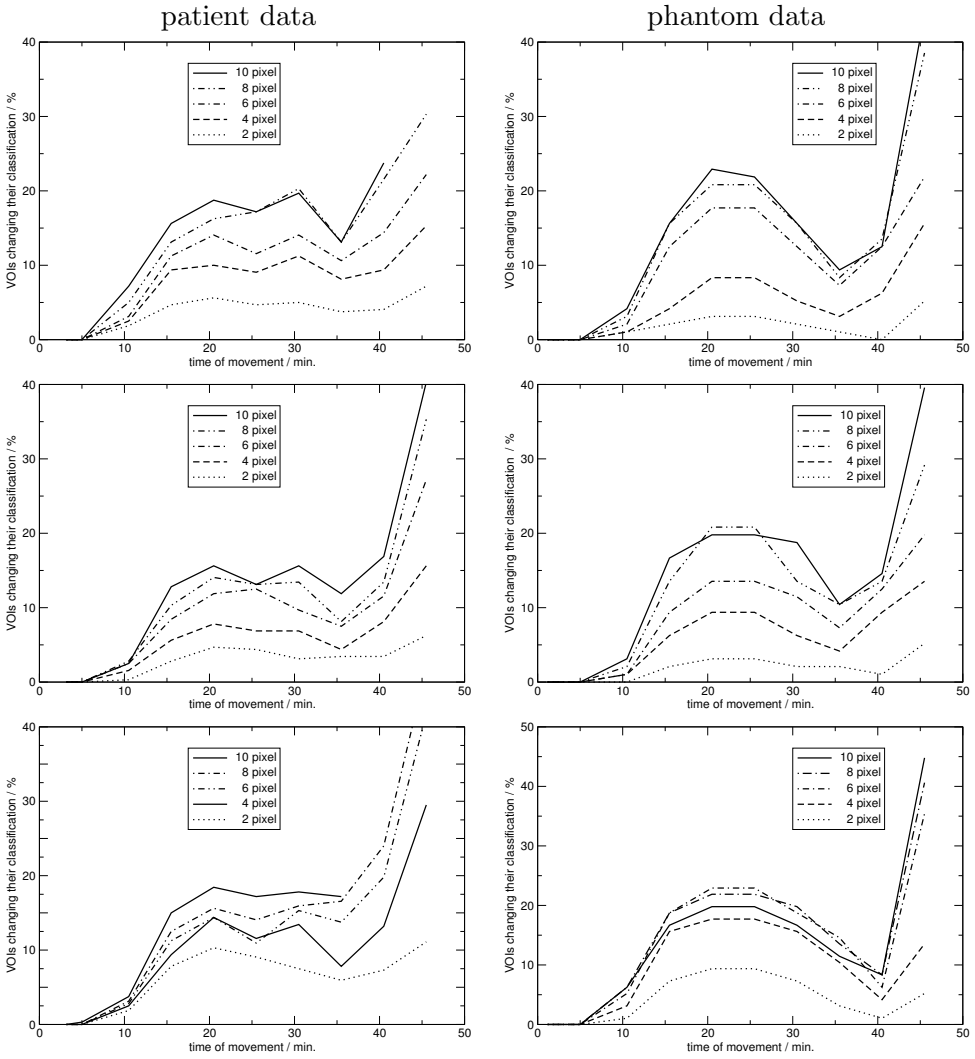

Figure 16: Effects of translation: x- (1. row), y- (2. row), and z-direction (3. row), all translations noted with their absolute value in the positive direction: left patient data, right phantom data

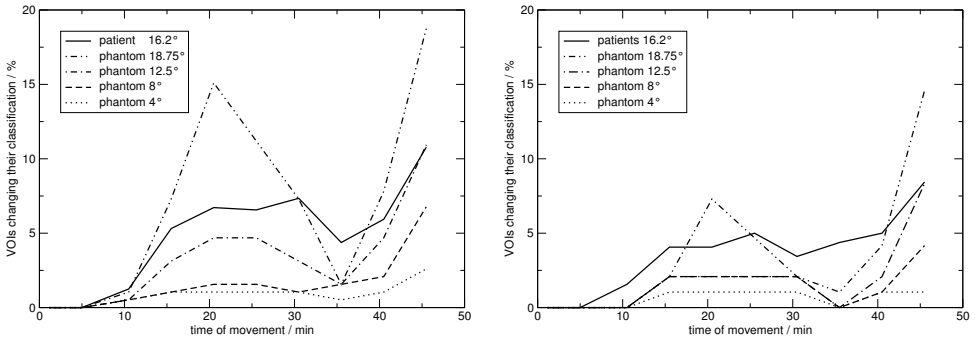

Figure 17: Effects of rotations around different axis: x'- and y'- (average left), and z-direction (right), all rotations noted with their absolute value in the positive direction: left patient data, right phantom data

5.3 Validation II: Simulation vs. Clinical Motion

Effects of motion on the classification of glucose metabolism on artificial moved data was compared to those in clinical data: movement in clinical data was registrated and corrected and effects on classification evaluated. Those effects were compared to effects on artifical moved datasets of the same absolute value, same main direction and same time point during acquisition (figure 18). Error bars in figure 18 for patient (PAM group) and phantom data are derived from the estimation of the time of movement: it could not be assigned to one point since most patients did not show a sudden movement but a distribution over adjacent planes. Error bars for the patient data (PCM group) are correlated to the sampling interval: one frame of 16 is related to be 6.25 % of the frames.

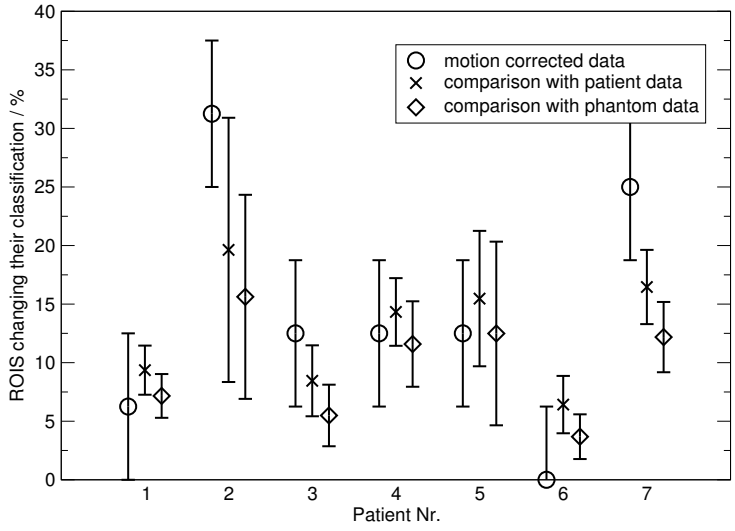

Figure 18: Effects of motion correction on classification of myocardial regions: ratio of corrected vs uncorrected patient data (PCM group) compared to artificial shifted patient (PAM group) and phantom data.

6 Discussion

6.1 Clinical Relevance: Motion Detection

Motion was clearly detected in 24 (= 38 %) patients (PCM group, figure 13). This incidence fulfilled the expectations, that due to longer acquisition times and better resolution of PET-systems motion is visible more frequently than in SPECT-acquisitions (17 - 25 % for cardiac ^{201}Tl-investigations [51, 5, 21, 20]). The rate of 38 % can be treated as lower limitation, since shifts up to 5 mm were assumed to be zero and the registration method operated only in counts of whole pixels. This result is supported by a PET study, where serious effects of motion on absolute quantified blood flow by means of

^{13}N-ammonia were achieved [41] but no rate of motion occurence was given.

The disadvantage of losing resolution in the registration process is compensated by leaving pixel-values in the original sampling and excluding biasing by resampling [1] which is important in this quantitative study.

6.2 Validation I: Simulation vs. Artificial Motion

6.2.1 Translation

General effects in figure 16 are similar for all directions and both simulations: motion effects increases with the amount of shift and contributes to the effects, only when occurring at least 5 min. after injection. Effects gain a local maximum and decrease at times up to 40 min to increase at later times. A kind of linearity with the amount of motion appears for motion up to 6 pixel, whereas larger shifts do not increase the VCC substantially, especially in phantom data.

The general trend can be explained, when considering a VOI falsely positioned due to patient motion is shifted to its right position after the time of movement. The right placement of a VOI inherits an increase of the value for the concentration of FDG in tissue $c_i^*(t)$ by a relative factor (see figure 14). Two effects are superpositioned:

1. The later the motion occurs, the fewer points lie on the right position and the higher is the effect: the slope is underestimated (see figure 14, right).

2. When assuming that the plasma concentration $c_p^*(t)$ being unbiased, the combined slope of the biased and unbiased part of the tissue concentration $c_i^*(t)$ is calculated. The slope is overestimated when patient motion occurs in the middle of the acquisition (see figure 14, left).

In patient motion events at acquisition times of 35 to 40 minutes both effects cancel out each other to a certain extent, resulting in the local minimum visible in patient and phantom data.

Saturation for large shift values effects can be explained by finding the VOI far outside the myocardium: shifting a software phantom with 200 mm myocardial thickness 8 pixels in (y, y-direction: 19.2 mm; z-direction: 25.6 mm) perpendicular to the epicardium, the VOI is placed outside the myocardium (nearly) in its whole. Shifting the VOI further 2 pixels at a constant input curve worsens the effect for the well defined phantom data only slightly. Patient data is more inhomogeneous: changes in VOI activity-concentrations can also occur far outside the VOI's original position so that motion effects are still visible.

The shape of a line profile of the myocardium seems to be a key parameter in software phantom simulation; the differences in shape are shown in figure 15. Comparing 3 patients with a thin myocardium selected from the PAM-group with the simulation of a phantom of 12.5 mm myocardial thickness similar results were achieved. These is explained easily when comparing at a fixed amount of shift the ratio between the correctly placed part of a VOI and the misaligned part relative to the myocardium. The ratio is higher

for a thin myocardium and can bias the VOI's activity-concentrations and hence glucose metabolism calculation more seriously. It can be concluded that motion effects depend strongly on the single dataset.

The comparison of patient group (PAM group) and phantom data reaches a limit at a certain amount of movement. One systematical reason additional to the saturation effect can be found in the different types of input curves used: input curves were generally achieved by placing VOIs in a blood pool region, atrium for patients and left ventricle for phantom data. Patient data was extracted from biased datasets whereby those for phantom data was taken as constant, like being derived with a blood sampling device [4, 62]. For the ranges of motions detected (up to 6 pixel) in clinical data both approaches did not show significant differences. The blood pool region of patient motion biased data will be shifted into the myocardium at higher shift levels and will affect the result of Patlak analysis more than a constant input curve. Furthermore, neighbouring organs (e.g. liver) might be stripped by the blood regions.

6.2.2 Rotation

Rotation was investigated in an artificial coordinate system which does not reflect common rotations of patient movement. The amount of translation from a rotational movement depends strongly on the distance between rotation centre and the left ventricle (see figure 10). Rotation centres can be assumed to be different from patient to patient. Independency of the effects

of rotational movement from the distance of rotation centre and left ventricle is achieved by the used coordinate system.

Rotations in this orientation have, generally spoken, smaller effects on the VCC than translations, particular rotations around the z'-axis. Behaviour of effects with time are similar to those observed with translational patient motion. Saturation effects are not observed. Comparison to patient data shows similar trends.

The lack of saturation can be explained since a rotational movement of a small amount will not displace a VOI totally from its correct placement: a further rotation will continously lead to further effects.

As the geometry of the left ventricle suggests, the rotational part of patient movement (seperated from a global patient movement according equation 8) does not affect the values for glucose metabolism seriously. The range of rotations presented seems to be quite high: simulated 2 h brain studies from 30 patients [45] showed rotations (sagittal plane: 0°-14° (mean 2.8°), transaxial plane: 1.5°-21° (mean 4.9°), coronal 0°) whereby only the behaviour of coronal plane might be compared with the constrained situation of the heart during a PET-acquisition. A rotation of 2° corresponds to approximately a 1 mm shift in a myocardium with the geometry of the presented phantom. Comparing rotational effects to those from translational movement they might be disregarded and the correction of patient movement only for the translational amount is justified.

6.3 Validation II: Simulation vs. Clinical Motion

Comparison of the effects of motion-correction on the absolute quantification showed similar results. The differences between patient-simulation (PAM group) and phantom-simulation are consistent with the relative differences in figure 18. Some discrepancies occurred especially in the two patients with large effects on the VCC. This is consistent with the conclusion, that motion effects depend strongly on the single dataset as reported in [41]. A prediction of the effect of patient motion on a single dataset is not possible: neither the comparison with the artificial moved patient data nor with the artificial moved software phantom would match firmly the single circumstances. In this comparison, software phantom data competes with artificially moved patient data (PAM group).

6.4 Limitations

The software phantom implies an idealisation of the anatomy and physiology of the heart. Results from the software phantom data cannot be transferred to clinical data without restrictions as explained above. Some reasons for the limitations of the presented approach and patient data are to be mentioned here:

- The activity level of each of the 16 heart regions can be set individually. In a human heart neighbouring regions are not as independent and the metabolic states do not differ like in phantom data. Shifting similar

regions into each other might cause lower effects

- The occurence of patient motion in phantom data was assumed to be sudden. On the other hand patient data often included motion occurence distributed over a few frames.

- Phantom data has a well-defined geometry with respect to myocardial thickness whereas patient data shows intra subject variations (e.g. papillary muscles).

- The orientation of the phantom heart is assumed to be 45° proned in each direction (x, y, z). Variations to these orientation might be found in reality. Inhomogeneity in different directions might be partly explained by this fact.

- The phantom heart is a quite symmetric body. Hence, especially for rotations around the z'-axis underestimated results occur.

- Transmissions scans were performed before the dynamic emission scans. This had no effect on the simulated movements, as motion was performed after transmission correction of the datasets. Motion correction of patient data was only applied to reconstructed datasets, where a misalignment between emission and transmission was present. Effects of discrepancies in correct alignment are known [52, 39].

- The motion registration approach used in this work is no "high-end"-procedure but a fast algorithm. It might not obtain the best achievable

results for motion registration. A review of state-of-the-art methods can be found in [28].

- Normally regions are drawn in the frames of a study, where anatomy is most visible; although a check for the right alignment of the regions might reduce the errors: if patient motion occurs the investigator might place the regions in the middle of these two regions, select smaller or wider regions, all biasing the result. If motion occurs in the last frames rejection of these would be a solution without motion correction.

- The movements in different directions and of different types might not be distributed similarly because the geometric limitations of patient movement due to the small aperture of a PET-scanner.

Taking these sources of errors into account, the presented results of the software phantom and the clinical datasets match each other in a satisfactory manner.

7 Conclusion

It has been shown that patient motion is a serious challenge in quantitative cardiac PET. It was determined that patient motion occurs in more than a third of the patients, a dedicated work on motion registration might detect even higher rates.

Influences of patient motion simulated in detail on a new developed fully dynamic cardiac software phantom could be applied to real data. No quantitative perfect match was achieved since simulation effects are strongly dependant of the geometry of the single patient or phantom myocardium. Nevertheless, general influences could be determined precisely. The model seems to be applicable to the investigation of various kinds of spatial influences (cardiac gating, respiratory gating) in quantitative cardiac PET.

Hybrid systems will not solve the discussed intra study motion problem in dynamic acquisitions since the acquisition of physiological data with PET and anatomical data is conducted separately and the static anatomical data set, that does not include any information about the patient motion.

Again the basic need for a reliable motion correction algorithm in the clinical routine was demonstrated.

8 Curriculum Vitae

Name	Jörg Joseph Eckardt
born	12.08.1971 in Münster
Parents	Heinz-Günther Eckardt, Waltraud Eckardt, geb. Meise
1977-1981	Elementary School in Münster
1981- 1990	Grammar School: Johann-Conrad-Schlaun Gymnasium Münster
23.05.1990	G.C.S.E. A-levels
1990-1997	Study of Physics: University of Münster
07.03.1997	Diploma. Work: “Optimierung von Geräteparametern für den Nachweis kleiner Teilchen in hochauflösenden Elementverteilungsbildern”
1997-1998	Civil Service at the Department of Nuclear Medicine, University of Münster
since 1998	Resarch fellow at the Department of Nuclear Medicine, University of Münster
1998-2000	Project manager for the installation and start-up of the cyclotron facility

Resarch Papers

- Franzius C, Bielack S, Flege S, Eckardt J, Sciuk J, Jürgens H, Schober O. High-activity samarium-153-EDTMP therapy followed by autologous peripheral blood stem cell support in unresectable osteosarcoma. Nuklearmedizin. 2001 Dec; 40(6): 215-20.

Abstracts

- Krämer KH, Redlich P, Eckardt J, Kohl H. Messung und Berechnung von Intensitätsprofilen in Elementverteilungsbildern von Nanoröhrchen im STEM. Optik 1997

- Eckardt J, Schäfers K, Lerch M, Schober O. Aufbau eine kostengünstigen Blutaktivitätsmessgerätes. Nuklearmedizin 1998; 37: V 6

9 Acknowledgements

Finally I want to thank all the persons who made this thesis possible:

At first I want to thank Prof. Dr. Dr. O. Schober for his continuous support for this work. He always gave me the freedom to work on this thesis.

Furtheron I want to thank Prof. Dr. M. Schäfers who has been a great help to me: he was always prepared for every discussion and provided me with very helpful suggestions.

A special thank is dedicated to Dr. K. Schäfers: without his detailed knowledge in PET-software and the access to his software for PET-modelling this work would not have been realizable in this way.

I am very grateful to Christine Bätza and especially Silke Steinhoff from the experimental group of our department for their help in the analysis of patient data. Alike I express my grace to Dipl. Ing. M. Kriens, T. Isokeit, Dr. C. Quentmeier and Dr. G. Lottes for the outstanding cooperative atmosphere during the daily work and all my colleagues from the the Department of Nuclear Medicine for their cooperative work and their patience with the occupation of computer capacity by me.

Last but not least I thank my sister Doris and my brother Wolfgang for their help in correcting this manuscript and all my friends and my family for their patience with me in times when work on this thesis occupied me.

References

[1] Andersson, JL: How to obtain high-accuracy image registration: application to movement correction of dynamic positron emission tomography data. In: *Eur J Nucl Med* 25 (1998), Nr. 6, S. 575–86

[2] Bergstrom, M; Eriksson, L; Bohm, C; Blomqvist, G; Litton, J: Correction for scattered radiation in a ring detector positron camera by integral transformation of the projections. In: *J Comput Assist Tomogr* 7 (1983), Nr. 1, S. 42–50

[3] Blokland, JA; Trindev, P; Stokkel, MP; Pauwels, EK: Positron emission tomography: a technical introduction for clinicians. In: *Eur J Radiol* 44 (2002), Nr. 1, S. 70–5

[4] Boellaard, R; van Lingen A; van Balen SC; Hoving, BG; Lammertsma, AA: Characteristics of a new fully programmable blood sampling device for monitoring blood radioactivity during PET. In: *Eur J Nucl Med* 28 (2001), Nr. 1, S. 81–9

[5] Botvinick, EH; Zhu, YY; O'Connell, WJ; Dae, MW: A quantitative assessment of patient motion and its effect on myocardial perfusion SPECT images. In: *J Nucl Med* 34 (1993), Nr. 2, S. 303–10

[6] Brown, E; Dairiki, JM; Doebler, RE; Lederer, CM (Hrsg.); Shirley, VS (Hrsg.): *Table of Isotopes*. New York : Wiley-Interscience, 1978

[7] Brown, TF; Yasillo, NJ: Radiation safety considerations for PET centers. In: *J Nucl Med Technol* 25 (1997), Nr. 2, S. 98–102; quiz 104–5

[8] Casey, ME; Gadagkar, H; Newport, D: A component based method for normalisation in volume pet. In: *Proceedings of the 3rd International Meeting on Fully Three-Dimensional Image Reconstruction in Radiology and Nuclear Medicine, Aix-les-Bains* (1995)

[9] Casey, ME; Nutt, R: Multicrystal two dimensional bgo detector system for positron emission tomography. In: *IEEE Trans Nucl Sci* 33 (1986), S. 460–463

[10] Chen, K; Bandy, D; Reiman, E; Huang, SC; Lawson, M; Feng, D; Yun, LS; Palant, A: Noninvasive quantification of the cerebral metabolic rate for glucose using positron emission tomography, 18F-fluoro-2-deoxyglucose, the Patlak method, and an image-derived input function. In: *J Cereb Blood Flow Metab* 18 (1998), Nr. 7, S. 716–23

[11] Cho, S; McConnell, MV: Echocardiographic and magnetic resonance methods for diagnosing hibernating myocardium. In: *Nucl Med Commun* 23 (2002), Nr. 4, S. 331–9

[12] Cooper, JA; Neumann, PH; McCandless, BK: Effect of patient motion on tomographic myocardial perfusion imaging. In: *J Nucl Med* 33 (1992), Nr. 8, S. 1566–71

[13] DeFronzo, RA; Tobin, JD; Andres, R: Glucose clamp technique: a method for quantifying insulin secretion and resistance. In: *Am J Physiol* 237 (1979), Nr. 3, S. E214–23

[14] DePuey, EG; Garcia, EV: Optimal specificity of thallium-201 SPECT through recognition of imaging artifacts. In: *J Nucl Med* 30 (1989), Nr. 4, S. 441–9

[15] Eckardt, J; Schober, O: Strahlenschutz in der Positronen-Emissions- Tomographie (PET). In: *Strahlenschutz* 9 (2002), S. 6–13

[16] Eisner, R; Churchwell, A; Noever, T; Nowak, D; Cloninger, K; Dunn, D; Carlson, W; Oates, J; Jones, J; Morris, D; et al.: Quantitative analysis of the tomographic thallium-201 myocardial bulls-eye display: critical role of correcting for patient motion. In: *J Nucl Med* 29 (1988), Nr. 1, S. 91–7

[17] Eisner, RL: Sensitivity of SPECT thallium-201 myocardial perfusion imaging to patient motion. In: *J Nucl Med* 33 (1992), Nr. 8, S. 1571–3

[18] Eisner, RL; Noever, T; Nowak, D; Carlson, W; Dunn, D; Oates, J; Cloninger, K; Liberman, HA; Patterson, RE: Use of cross-correlation function to detect patient motion during SPECT imaging. In: *J Nucl Med* 28 (1987), Nr. 1, S. 97–101

[19] Fitzgerald, J; Danias, PG: Effect of motion on cardiac SPECT imaging: recognition and motion correction. In: *J Nucl Cardiol* 8 (2001), Nr. 6, S. 701–6

[20] Friedman, J; Berman, DS; Van Train, K; Garcia, EV; Bietendorf, J; Prigent, F; Rozanski, A; Waxman, A; Maddahi, J: Patient motion in thallium-201 myocardial SPECT imaging. An easily identified frequent source of artifactual defect. In: *Clin Nucl Med* 13 (1988), Nr. 5, S. 321–4

[21] Friedman, J; Van Train, K; Maddahi, J; Rozanski, A; Prigent, F; Bietendorf, J; Waxman, A; Berman, DS: "Upward creep" of the heart: a frequent source of false-positive reversible defects during thallium-201 stress-redistribution SPECT. In: *J Nucl Med* 30 (1989), Nr. 10, S. 1718–22

[22] Gambhir, SS; Czernin, J; Schwimmer, J; Silverman, DH; Coleman, RE; Phelps, ME: A tabulated summary of the FDG PET literature. In: *J Nucl Med* 42 (2001), Nr. 5 Suppl, S. 1S–93S

[23] Gambhir, SS; Schwaiger, M; Huang, SC; Krivokapich, J; Schelbert, HR; Nienaber, CA; Phelps, ME: Simple noninvasive quantification method for measuring myocardial glucose utilization in humans employing positron emission tomography and fluorine-18 deoxyglucose. In: *J Nucl Med* 30 (1989), Nr. 3, S. 359–66

[24] Gonzalez, L; Vano, E; Cordeiro, CA; Carreras, JL: Preliminary safety evaluation of a cyclotron facility for positron emission tomography imaging. In: *Eur J Nucl Med* 26 (1999), Nr. 8, S. 894–9

[25] Hill, DL; Batchelor, PG; Holden, M; Hawkes, DJ: Medical image registration. In: *Phys Med Biol* 46 (2001), Nr. 3, S. R1–45

[26] Huang, SC; Phelps, ME; Hoffman, EJ; Sideris, K; Selin, CJ; Kuhl, DE: Noninvasive determination of local cerebral metabolic rate of glucose in man. In: *Am J Physiol* 238 (1980), Nr. 1, S. E69–82

[27] Huesman, RH; Klein, GJ; Reutter, BW; Coxson, PG; Botvinick, EH; Budinger, TF: Strategies for extraction of quantitative data from volumetric dynamic cardiac positron emission tomography data. In: *Cardiology* 88 (1997), Nr. 1, S. 54–61

[28] Hutton, BF; Braun, M; Thurfjell, L; Lau, DH: Image registration: an essential tool for nuclear medicine. In: *Eur J Nucl Med* 29 (2002), Nr. 4, S. 559–77

[29] Kinahan, PE; Townsend, DW; Beyer, T; Sashin, D: Attenuation correction for a combined 3D PET/CT scanner. In: *Med Phys* 25 (1998), Nr. 10, S. 2046–53

[30] Klein, C; Nekolla, SG; Bengel, FM; Momose, M; Sammer, A; Haas, F; Schnackenburg, B; Delius, W; Mudra, H; Wolfram,

D; Schwaiger, M: Assessment of myocardial viability with contrast-enhanced magnetic resonance imaging: comparison with positron emission tomography. In: *Circulation* 105 (2002), Nr. 2, S. 162–7

[31] Knoll, GF: *Radiation Detection and Measurement*. United States : Wiley, 1989

[32] Knuuti, MJ; Nuutila, P; Ruotsalainen, U; Saraste, M; Harkonen, R; Ahonen, A; Teras, M; Haaparanta, M; Wegelius, U; Haapanen, A; et al.: Euglycemic hyperinsulinemic clamp and oral glucose load in stimulating myocardial glucose utilization during positron emission tomography. In: *J Nucl Med* 33 (1992), Nr. 7, S. 1255–62

[33] Lawrence, EO; Livingston, MS: The Production of High Speed Light Ions without the Use of High Voltages. In: *Phys. Rev.* 40 (1932), S. 19–37

[34] Levin, CS; Hoffman, EJ: Calculation of positron range and its effect on the fundamental limit of positron emission tomography system spatial resolution. In: *Phys Med Biol* 44 (1999), Nr. 3, S. 781–99

[35] Luss, H; Schafers, M; Neumann, J; Hammel, D; Vahlhaus, C; Baba, HA; Janssen, F; Scheld, HH; Schober, O; Breithardt, G; Schmitz, W; Wichter, T: Biochemical mechanisms of hibernation

and stunning in the human heart. In: *Cardiovasc Res* 56 (2002), Nr. 3, S. 411–21

[36] Maintz, JB; Viergever, MA: A survey of medical image registration. In: *Med Image Anal* 2 (1998), Nr. 1, S. 1–36

[37] Mazur, W; Nagueh, SF: Myocardial viability: recent developments in detection and clinical significance. In: *Curr Opin Cardiol* 16 (2001), Nr. 5, S. 277–81

[38] McCarthy, TJ; Welch, MJ: The state of positron emitting radionuclide production in 1997. In: *Semin Nucl Med* 28 (1998), Nr. 3, S. 235–46

[39] McCord, ME; Bacharach, SL; Bonow, RO; Dilsizian, V; Cuocolo, A; Freedman, N: Misalignment between PET transmission and emission scans: its effect on myocardial imaging. In: *J Nucl Med* 33 (1992), Nr. 6, S. 1209–14; discussion 1214–5

[40] Montalescot, G; Faraggi, M; Drobinski, G; Messian, O; Evans, J; Grosgogeat, Y; Thomas, D: Myocardial viability in patients with Q wave myocardial infarction and no residual ischemia. In: *Circulation* 86 (1992), Nr. 1, S. 47–55

[41] Muzik, O; Beanlands, R; Wolfe, E; Hutchins, GD; Schwaiger, M: Automated region definition for cardiac nitrogen-13-ammonia PET imaging. In: *J Nucl Med* 34 (1993), Nr. 2, S. 336–44

[42] O'Connor, MK; Kanal, KM; Gebhard, MW; Rossman, PJ: Comparison of four motion correction techniques in SPECT imaging of the heart: a cardiac phantom study. In: *J Nucl Med* 39 (1998), Nr. 12, S. 2027–34

[43] Ollinger, JM: Model-based scatter correction for fully 3d pet. In: *Phys Med Biol* 41 (1996), S. 153–176

[44] Patlak, CS; Blasberg, RG; Fenstermacher, JD: Graphical evaluation of blood-to-brain transfer constants from multiple-time uptake data. In: *J Cereb Blood Flow Metab* 3 (1983), Nr. 1, S. 1–7

[45] Patterson, H; Clarke, GH; Guy, R; McKay, WJ: Head movement in normal subjects during simulated brain imaging. In: *J Nucl Med Technol* 26 (1998), Nr. 4, S. 257–61

[46] Pereira, RS; Prato, FS; Wisenberg, G; Sykes, J; Yvorchuk, KJ: The use of Gd-DTPA as a marker of myocardial viability in reperfused acute myocardial infarction. In: *Int J Cardiovasc Imaging* 17 (2001), Nr. 5, S. 395–404

[47] Phelps, ME; Hoffman, EJ; Selin, C; Huang, SC; Robinson, G; MacDonald, N; Schelbert, H; Kuhl, DE: Investigation of [18F]2-fluoro-2-deoxyglucose for the measure of myocardial glucose metabolism. In: *J Nucl Med* 19 (1978), Nr. 12, S. 1311–9

[48] Picard, Y; Thompson, CJ: Motion correction of PET images using multiple acquisition frames. In: *IEEE Trans Med Imaging* 16 (1997), Nr. 2, S. 137–44

[49] Pike, VM: The Status of PET Radiochmeistry for Drug Development and Evaluation. In: *Drug Inf J* 31 (1997), S. 997–1013

[50] Pinto, FJ: Myocardial viability: the search for a perfect method is not over yet. In: *Eur Heart J* 21 (2000), Nr. 13, S. 1039–40

[51] Prigent, FM; Hyun, M; Berman, DS; Rozanski, A: Effect of motion on thallium-201 SPECT studies: a simulation and clinical study. In: *J Nucl Med* 34 (1993), Nr. 11, S. 1845–50

[52] Reinartz, P; Zimny, M; Cremerius, U; Sabri, O; Kaiser, HJ; Nowak, B; Bull, U: [Quantification of repositioning errors in PET studies through superimposition of emission and transmission scans. Comparison between acquisition with and without repositioning]. In: *Nuklearmedizin* 38 (1999), Nr. 6, S. 192–8

[53] Rigo, P; Van Boxem, P; Foulon, J; Safi, M; Engdahl, J; Links, J: Quantitative evaluation of a comprehensive motion, resolution, and attenuation correction program: initial experience. In: *J Nucl Cardiol* 5 (1998), Nr. 5, S. 458–68

[54] Sawada, S: Dobutamine echocardiography for detection of viable myocardium in ischemic cardiomyopathy. In: *Echocardiography* 17 (2000), Nr. 1, S. 69–77

[55] Schäfers, K: *Measurement of Myocardial Left Ventricular Volumes using Positron Emission Tomography and Radio-labelled Carbon Monoxide*, University of Muenster, Diss., 2000

[56] Slomka, PJ; Hurwitz, GA; Stephenson, J; Cradduck, T: Automated alignment and sizing of myocardial stress and rest scans to three-dimensional normal templates using an image registration algorithm. In: *J Nucl Med* 36 (1995), Nr. 6, S. 1115–22

[57] Sokoloff, L; Reivich, M; Kennedy, C; Des Rosiers, MH; Patlak, CS; Pettigrew, KD; Sakurada, O; Shinohara, M: The [14C]deoxyglucose method for the measurement of local cerebral glucose utilization: theory, procedure, and normal values in the conscious and anesthetized albino rat. In: *J Neurochem* 28 (1977), Nr. 5, S. 897–916

[58] Stöcklin, G (Hrsg.); Pike, VW (Hrsg.): *Radiopharmaceuticals for Positron Emission Tomography*. Kluwer Academic Press, 1993

[59] Strijckmans, K: The isochronous cyclotron: principles and recent developments. In: *Comput Med Imaging Graph* 25 (2001), Nr. 2, S. 69–78

[60] Svedlow, M; McGillem, CD; Anuta, PE: Image Registration: Similarity Measure and Preprocessing Method Comparisons. In: *IEEE T AERO ELEC SYS* 14 (1977), Nr. 1, S. 141–149

[61] Thompson, CJ; Dagher, A; Lunney, DN; Strother, SC; Evans, AC: A technique to reject scattered radiation in pet transmission scans. In: *Wkshp. Phys. Eng. Computerised Multidimensional Imag. Processing* 671 (1986), S. 244–253

[62] Votaw, JR; Shulman, SD: Performance evaluation of the Pico-Count flow-through detector for use in cerebral blood flow PET studies. In: *J Nucl Med* 39 (1998), Nr. 3, S. 509–15

[63] Wienhard, K; Eriksson, L; Grootoonk, S; Casey, M; Pietrzyk, U; Heiss, WD: Performance evaluation of the positron scanner ECAT EXACT. In: *J Comput Assist Tomogr* 16 (1992), Nr. 5, S. 804–13

[64] Wijns, W; Vatner, SF; Camici, PG: Hibernating myocardium. In: *N Engl J Med* 339 (1998), Nr. 3, S. 173–81

[65] Xu, M; Cutler, PD; Luk, WK: Adaptive, segmented attenuation correction for whole-body pet imaging. In: *IEEE Trans Nucl Sci* 43 (1996), S. 331–336

[66] Zaidi, H: Comparative evaluation of scatter correction techniques in 3D positron emission tomography. In: *Eur J Nucl Med* 27 (2000), Nr. 12, S. 1813–26

[67] Zoghbi, WA: Evaluation of myocardial viability with contrast echocardiography. In: *Am J Cardiol* 90 Suppl 10A (2002), S. 65J–71J